Pattern formation in drying drops

Robert D. Deegan*

James Franck Institute, 5640 South Ellis Avenue, Chicago, Illinois 60637

(Received 24 November 1998)

Ring formation in an evaporating sessile drop is a hydrodynamic process in which solids dispersed in the drop are advected to the contact line. After all the liquid evaporates, a ring-shaped deposit is left on the substrate that contains almost all the solute. Here I show that the drop itself can generate one of the essential conditions for ring formation to occur: contact line pinning. Furthermore, I show that when self-induced pinning is the only source of pinning an array of patterns—that include cellular and lamellar structures, sawtooth patterns, and Sierpinski gaskets—arises from the competition between dewetting and contact line pinning.

I. INTRODUCTION

A fluid droplet on a solid surface is ostensibly so simple a physical system that one might suppose that all its behavior is thoroughly understood. Despite countless studies going back at least 200 years [1], issues about the phenomena occurring at the contact line, defined as the line beyond which the solid is wet, continue to engage the interest of the scientific and engineering communities. One such issue is contact line pinning [2,3]. Looking through a window after a rainstorm, one is struck by the fact that droplets, though on a vertical surface, nonetheless defy gravity. The force that holds them in place arises from a pinning of the contact line by irregularities, such as roughness or chemical heterogeneity, on the surface of the glass [4]. Here I explore how the contact line can become pinned due to solute within the liquid that corrupts the substrate. The capacity of solute to alter the surface properties of the substrate is well known. However, in ring-forming drops it achieves a new scale in strength because the solute preferentially accumulates at the contact line, where it exterts the greatest influence on the motion of the contact line.

This work is an extension of an earlier study in which my colleagues and I developed and experimentally tested a theory for the formation of rings in drying drops [5,6]. A common manifestation of this phenomenon is the brown ring left when a drop of coffee dries on a counter top [see Fig. 1(a)]. We found that contact line pinning and evaporation are sufficient conditions for ring formation. Since these are common and generic conditions, ring formation often occurs whenever a liquid with solid constituents evaporates. The ring forms because the contact line cannot move. Therefore, when evaporation removes liquid from around the contact line, a flow develops to keep the substrate wet up to that point [see Fig. 1(b)]. The solute in the drop is dragged to the contact line by this flow, where it accumulates to form the ringlike deposit that remains after all the liquid evaporates.

The substrate by itself cannot keep the contact line pinned indefinitely. In Refs. [5,6] we speculated that the accumulation of solid components at the contact line perpetuates the

pinning of the contact line. Here I will refer to this process as ''self-pinning'' because of the bootstrapping that would be intrinsic to ring formation: some preexisting conditions on the substrate temporarily anchors the contact line; this permits the ring to start growing, and the additional growth increases the energy barrier the contact line must surmount before moving. In this paper I will show that self-pinning does occur, and that it gives rise to pattern formation.

II. SELF-PINNING

In order to test the hypothesis of self-pinning, I isolated the effects of solute pinning by using a smooth homogenous substrate. Freshly cleaved mica provides such a surface. The substrates were prepared from a slab of mica by prying open a corner and introducing a drop of deionized water. The water cleaves the interlayer potassium bond, and if done properly produces an atomically flat surface. In order to minimize contamination of the surface, the amount of water used during the cleaving process was kept as low as possible. The sheets were dried in open air (this typically took less than 20 s), briefly exposed to the flame of a Bunsen burner, and placed on a copper plate to cool. The sheets were used as soon as their temperature returned to normal.
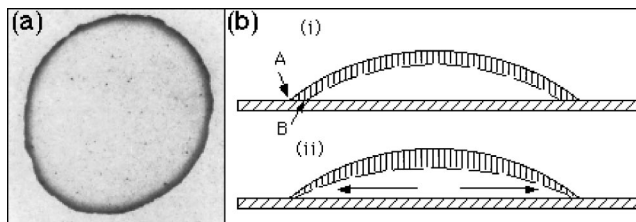

FIG. 1. (a) A photograph of a dried coffee drop. The dark perimeter is produced by a dense accumulation of coffee particles. The radius is approximately 5 cm. (b) Schematic illustration of the origin of the advective current. (i) If the contact line were not pinned, uniform evaporation would remove the hashed layer, the interface would move from the solid line to the dashed line, and the contact line would move from A to B. However, if the contact line is pinned then the retreat from A to B is not possible, and there must be a flow that replenishes the lost fluid. (ii) Shows the actual motion of the interface and the compensating current.

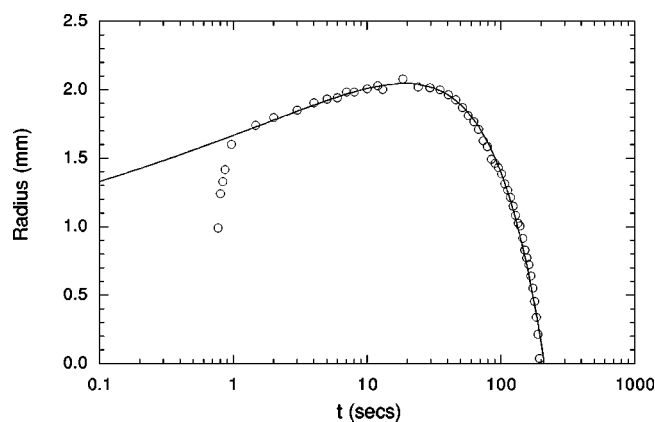*Electronic address: rddeegan@chaos.ph.utexas.edu

FIG. 2. Plot of the radius of a water drop (mm) drying on a mica substrate vs time.

Observations of the behavior of filtered deionized water deposited on the mica attest to smoothness and homogeneity of the substrate. (As with all fully wetting liquids, in addition to the macroscopic contact line there is also a microscopic line due to the precursor film that extends beyond the macroscopic contact line. The contact line referred to herein will always be the macroscopic contact line.) A drop with an initial volume of 0.5 μl was placed on the mica substrate, and its radius versus time was recorded. These data are plotted in Fig. 2. Initially the drop grew until reaching a maximum radius of 2 mm, and thereafter it shrank continuously to zero size. The smoothness of the data in Fig. 2 is a measure of the smoothness of the substrate. Repeated trials indicated that the substrates contained approximately one pinning site per cm^2.

The drops in the experiments that follow were made from a 2% solid volume fraction colloidal suspension of sulfate-terminated polystyrene microspheres dyed yellow-green fluorescent acquired from Interfacial Dynamics, Portland, Oregon. The colloid was synthesized by a surfactant-free method which minimizes the presence of amphiphilic molecules. I used two different microsphere diameters: 1 and 0.1 μm. Volume fractions different from 2% were made by diluting the colloid with deionized water, or by sedimenting the microspheres in a centrifuge and decanting the clear liquid.

When placed on mica, a drop of colloid will grow quickly to its largest size, much like the drop of pure water shown in Fig. 2. Unlike with pure water, the drop of colloid remains at its maximum size for a substantial fraction of the drying time. Nadkarni and Garoff [7] showed that a single microsphere attached to the surface can pin the contact line. The same process doubtlessly occurs here but at a much stronger level; the microspheres jam into the wedge of fluid next to the contact line, preventing it from retracting. A ring is formed during this initial pinned stage. At late times, the liquid pulls away from the ring and shrinks down to zero radius. During this phase, segments of the contact line continually switch between a pinned state and a depinned state, leaving a trail of deposits which can be highly regular. The depinning process begins with the nucleation of a dry spot along the inner edge of the ring (see Fig. 3). Gradually more dry spots develop until the contact between the liquid and the ring is completely severed. I measured the fraction of time
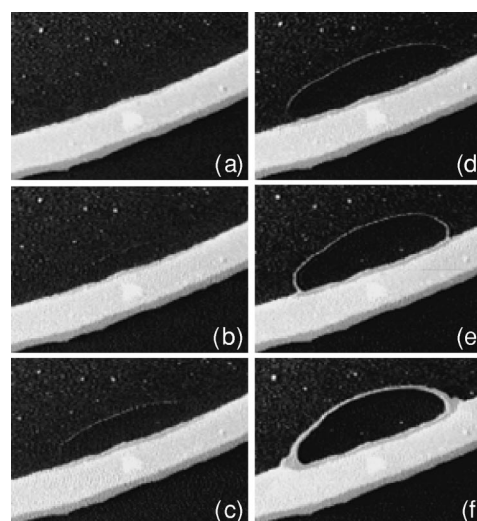

FIG. 3. Photographic sequence demonstrating the formation of a hole. The view is from above, and the solid white band in the lower part of the frame is the ring; the rest of the drop is above the ring. The hole is created, expands, and is eventually contained by the accumulation of microspheres along its edge. The portion of the ring next to the hole remains wet throughout the period covered by the figure. The flow inside the drop remains outward directed even when the contact line is retreating. (The backward motion of some of the larger particles appears to contradict this statement. However, these particles are clamped between the liquid surface and the substrate so that their motion is governed by the the interface's motion, and hence by the contact line's motion, instead of by the fluid flow.) The times for frames (a)–(f) are $t=0$, 0.23, 0.50, 0.83, 1.87, and 5.90 s, respectively. The major axis of the hole is approximately 150 μm.

during which the drop remained pinned and the width of the thinnest portion of the ring.

To measure the time of the initial pinned state, the drop was dried on an analytical balance and the mass as a function of time was recorded. A magnified image of the drop was acquired using a CCD camera, and was used to visually monitor the state of the drop. The depinning time t_d was measured when the first hole forms. The effective total drying time of the drop, t_f, was determined by a linear extrapolation of the mass versus time plot to zero, as shown in Fig. 4(a). Since the evaporation rate depends only on the radius of the drop, t_f is equal to the total drying time that would be obtained if the drop remained pinned throughout its lifetime. The depinning time, normalized by t_f, versus the initial solid volume fraction ϕ, is plotted in Fig. 4(b). The data are approximately linear on a log-log scale, and a best fit to a power law yields an exponent of 0.26 ± 0.08. For concentrations below 0.1% there was insufficient contrast in the video image of the drop to determine the depinning time.

The self-pinning process was also characterized by measuring as a function of initial concentration the width of the ring at its narrowest point. When a depinning event occurs the ring at that point ceases to grow, and so the thinnest portion of the ring indicates where the first depinning event occurred. The volume of each drop varied because of inaccuracies intrinsic to pipetting small volumes. Therefore, the width of the ring, w_d, was normalized by the drop radius R to compensate for different size drops. Figure 5(a) shows a
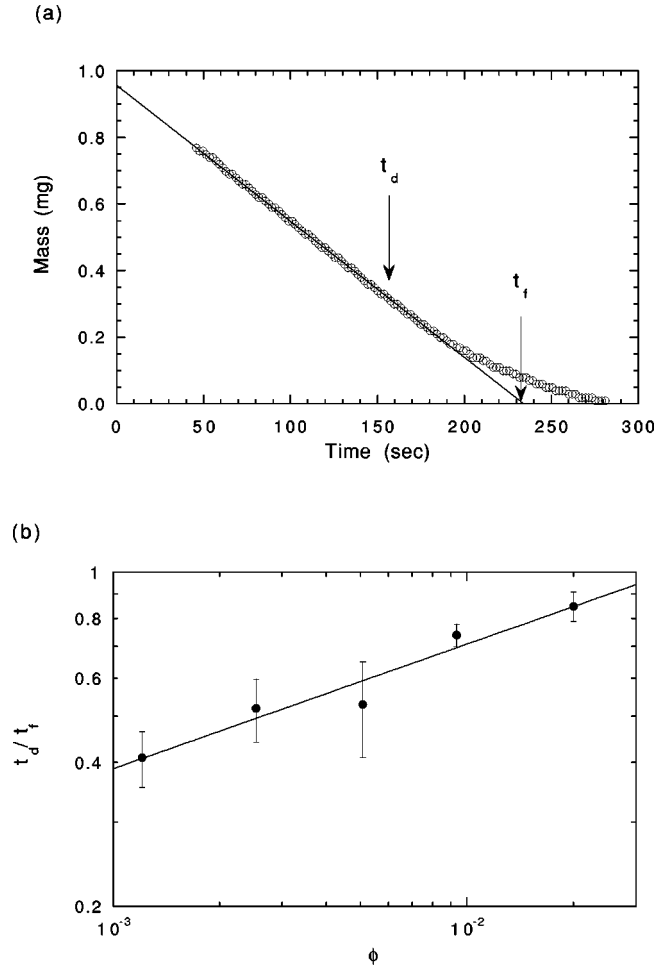
(a)

(b)

FIG. 4. (a) Mass of a drying drop vs time. The early time data are suppressed because it contains transients due to the settling time of the balance. The arrows indicate the depinning time, labeled t_d, and the extrapolated drying time, labeled t_f. The depinning time is determined by the first appearance of a hole, as in Fig. 3, near the contact line. (b) Depinning time normalized by the extrapolated drying time vs concentration. The line running through the data is a best-fit to a power law, which yields an exponent of 0.26 ± 0.08.

plot of w_d/R versus ϕ. For drops of equal volume the average radius maximum showed a slight concentration dependence, increasing by about 10% when the concentration changed by a factor of 10. The different data sets plotted correspond to 0.1- and 1-μm particle sizes. The two data sets coincide and, therefore, for clarity they are offset from each other by multiplying the 0.1-μm data by a factor of 5. I was unable to obtain data for particle sizes outside of this range because larger particles sediment too quickly and smaller particles are commercially unavailable in a surfactant-free suspension. Both data sets are well fit by a power law which for the 0.1-μm beads gives an exponent of 0.78 ± 0.10 and which for the 1-μm beads gives an exponent of 0.86 ± 0.10. Within the experimental uncertainty these two exponents are equal.

If changing the size of the drop only changes its scale and not its shape, then the width of the ring should scale with the radius. That is, the volume of the wedge-shaped ring will be proportional to Rw^2, and this volume must contain an amount of solute proportional to volume of the drop R^3 so
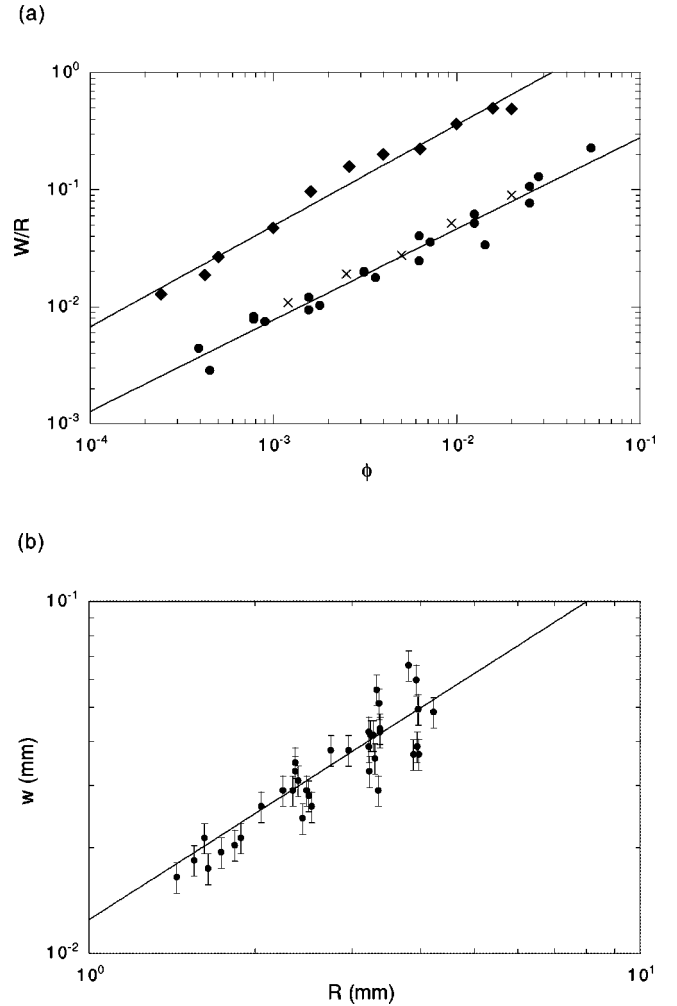
(a)

(b)

FIG. 5. (a) The width of the ring at depinning normalized by the drop radius vs the concentration. The upper data set is for the 0.1-μm microspheres, and the lower one is for the 1-μm microspheres. The 0.1-μm data set has been multiplied by 5 to separate the two data sets. A best fit to a power law gives an exponent of 0.78 ± 0.10 for the 0.1-μm microspheres and 0.86 ± 0.10 for the 1-μm microspheres. The crosses ($\times$) correspond to the width calculated using the model given in the Appendix and using the data from Fig. 4(b). (b) The width at depinning for drops of different sizes but of equal initial concentration (1.56×10^{-3} volume fraction) plotted against the radius. The line running through the data is a fit to the functional form $w = aR$.

that $w \propto R$. To explicitly test this assumption, I measured w_d and R for drops of different sizes but the same concentration. The results plotted in Fig. 5(b) demonstrate that the w_d scales with R over this range of radii.

It is not readily apparent that the width data of Fig. 5 are consistent with the depinning time data of Fig. 4. A rough estimate of the width as a function of time can be obtained by assuming that the ring is an annulus with a cross section shaped like a right triangle (i.e., a wedge). Therefore, its volume is

$$V_r = \pi R w^2 \theta_c, \tag{1}$$

with the approximation that $\tan \theta_c \simeq \theta_c$ which applies to the thin drops in my experiments. In prior work [6], the volume of the ring, V_r, as a function of time was shown to be

$$V_r = p^{-1} \frac{\pi R^3 \theta_c}{4} \phi [1 - (1 - t/t_f)^{3/4}]^{4/3}, \qquad (2)$$

where the prefactor is the total amount of solute in the drop at $t=0$ multiplied by the inverse of the packing fraction, p. The formula indicates that initially there is no ring [$V_r(t=0)=0$], and that the final ring contains all the solute. Combining Eqs. (1) and (2) produces

$$w/R = \sqrt{\frac{\phi}{4p}} [1 - (1 - t/t_f)^{3/4}]^{2/3} \sim \sqrt{\phi} t^{2/3} \qquad (3)$$

for $t \ll t_f$. At the first depinning event $w_d = w(t_d) \sim \sqrt{\phi} t_d^{2/3}$. Using the experimental result $t_d \sim \phi^{0.26 \pm 0.08}$ yields $w_d \sim \phi^{0.67 \pm 0.05}$. This result is consistent within experimental uncertainty with the width data of 0.1-μm microspheres but not with the width data of the 1-μm microspheres.

Equation (3) underestimates the growth rate of the ring because the ring's actual shape is different from that of a wedge. Consider the innermost edge of the ring to be the interface between a solid (packed microspheres) and a liquid. The speed with which the interface moves inward is determined by how fast microspheres arrive and how highly they can be stacked. The height of the stacking depends on the angle of the liquid surface relative to the substrate; a larger angle can accommodate a higher stacking of microspheres. Since this angle must be smaller than the initial contact angle and is, furthermore, decreasing in time, the ring will be wider than that calculated above. A more precise calculation for the ring width which explicitly includes the opening angle is given in the Appendix. For each of the data points (ϕ, t_d) in Fig. 4(b), the differential equations in the Appendix were numerically integrated from $t=0$ through $t=t_d$, using ϕ as an input parameter. The crosses in Fig. 5(a) correspond to the results of this integration. The agreement between the depinning time and width data is good.

These experimental results demonstrate that self-pinning does occur and that it has a predictable dependence on the initial concentration. It is worth emphasizing that contact line pinning due to the accumulation of microspheres is expected and has already been amply demonstrated by Nadkarni and Garoff [7]. What is unusual about the pinning process in this system is that it arises from a self-organization of the pinning sites.

The formation of a hole is the first stage of depinning. A subset of possible mechanisms for its formation are dynamical instabilities. In order to determine the relevance of kinetic effects, I reduced the rate of evaporation so that dynamical quantities such as flow velocity and temperature gradients were reduced. To accomplish this, a drop was placed on a mica substrate and covered with a microscope slide in which a bowl about 2 cm wide and 2 mm deep was carved out. The drop was thus surrounded by a glass container which vented to the atmosphere solely through the gaps between the glass slide and the substrate. The drop took 20 times longer to dry than an identical drop drying in the open air. I found that the first hole appeared in the slow drying drop at the same effective time, t/t_f, as its rapidly drying counterpart. I therefore concluded that hole formation is not a dynamical effect (see Fig. 6).
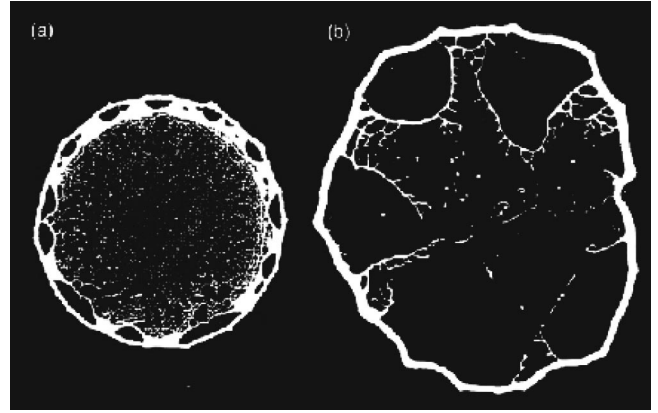

FIG. 6. (a) The deposit left by a drop dried in the open air. (b) The deposit left by a drop, made from the same solution as (a), dried in the chamber described in text. The drying time is 20 times longer for (b) than for (a). The images have the same scale and so the photographs indicate that (b) is approximately twice as wide as (a). This is the result of the drop in (b) spreading for a longer time period than (a) before evaporation truncated the spreading process. Also, the images indicate that the sizes of the arches in (b) are much larger than those in (a). The diameter of the deposit in (a) is approximately 5 mm. The scales in (a) and (b) are the same.

The apparent lack of a dynamic signature at the onset of hole formation leaves open the possibility of a static criterion. The spontaneity with which holes form is reminiscent of nucleation and growth phenomenon. This suggests a static criterion might be based on energetic considerations. However, the ingredients in the energy balance are unclear, considering that the depinning in a ring-forming drop is unusual in several respects. First, though the free energy of a water drop will decrease as it spreads over mica, the retraction shown in Fig. 2 is what one would expect if spreading were energetically unfavorable. In other words, though water wets mica it behaves as if though it were only partially wetting. Second, the depinning of a contact line from a surface asperity only involves a distortion of the contact line whereas the depinning in a ring-forming drops involves the creation of a new contact line. Third, though the hole clearly has a macroscopic contact line, the region within the hole is coated with a thin layer of liquid, i.e., the precursor film. Any explanation of the depinning must account for these effects.

Using the data of Fig. 5, I searched for a static criterion based on the geometrical proportions of the ring. I used the model in the Appendix to calculate the height of the ring, h, and the angle of the free surface with respect to the substrate, Θ. In Fig. 7(a), h versus ϕ is plotted. These data show that h is a strong function of ϕ. In Fig. 7(b), the h versus w is plotted. The data are well described by a power law to which a best-fit yields an exponent of 0.85 ± 0.05. Since $dh/dw \approx \Theta$ this indicates that $\Theta \sim w^{-0.15 \pm 0.05}$ which together with the dependence of w on ϕ gives $\Theta \sim \phi^{0.12 \pm 0.05}$. Since this is a weak function of ϕ, it appears that depinning occurs once Θ reaches some threshold value.

III. PATTERN FORMATION

The focus of Sec. II was the pinning force on the contact line exerted by the deposited solute. During this early stage
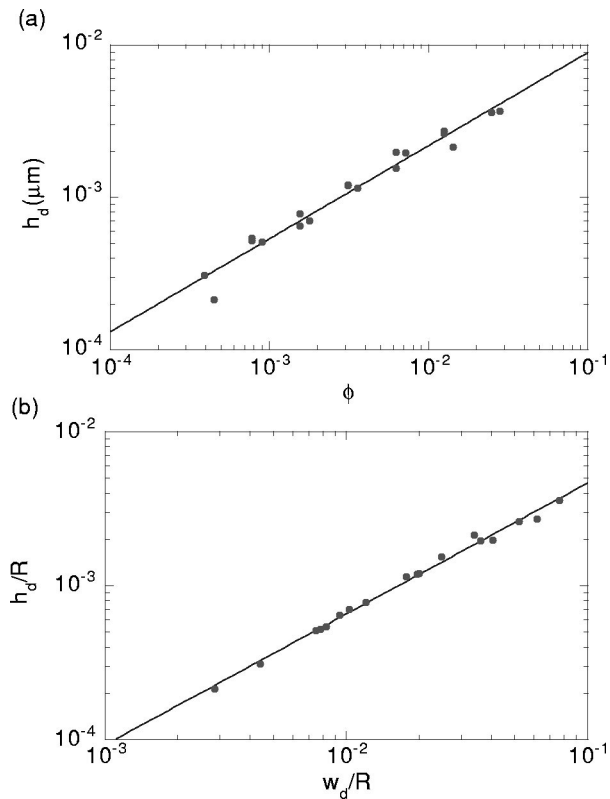
(a)

(b)

FIG. 7. (a) The height of the ring at depinning in units of μm calculated using the results of the Appendix and the data in Fig. 5. (b) The height at depinning vs w_d. The data are best fit by a power law with an exponent of 0.85 ± 0.05.

of the drop's life the pinning force is so large that it is solely responsible for the contact line behavior. Uncomplicated constraints produce simple structures: a ring. This section shifts the focus to the events that occur after the contact line separates from the ring. Dewetting [8] and pinning forces are of comparable strength during this stage. Here I will show that the competition between these two forces leads to complicated yet ordered behavior.

As in the self-pinning experiments, the observations that follow are of drops of colloidal microspheres drying on a freshly cleaved mica surface. (Experiments conducted using a cleaned, optically flat, silicon substrate gave similar results.) The additional step of briefly centrifuging the 0.1-μm sample before use was performed to remove large particles (~ 1 μm) because otherwise the resulting deposits were irreproducible. The experimental control parameters were particle size, solute concentration, surfactant concentration, ionic strength, and polydispersity of the particle size. All observations were done with the aid of a fluorescent microscope. Therefore, the gray level in the images that follow is proportional to the number of particles at a given point with white corresponding to the largest value.

A. Patterns with 0.1-μm particles

Arranged top to bottom in order of decreasing concentration, Fig. 8 shows the deposit resulting from dried drops of different initial concentration of 0.1-μm microspheres. The left-hand column shows a complete picture of the deposit, whereas the right-hand column shows only magnified frag-

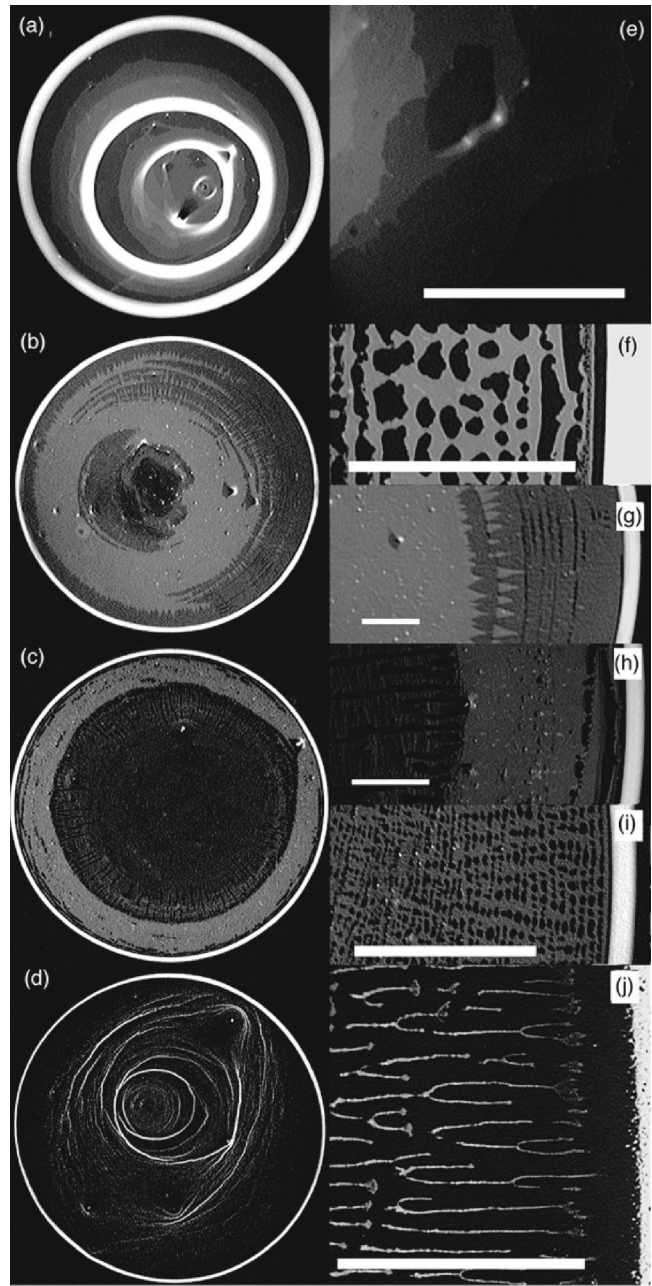FIG. 8. Photographs of the deposit left by drops containing 0.1-μm microspheres at various concentrations dried on mica. The grey scale indicates the density of particles in a given area with white corresponding to the highest value. The left column shows the entire deposit for initial volume fractions (a) 1%, (b) 0.25%, (c), 0.13%, and (d) 0.063%. The diameter of these drops is approximately 6 mm. The right column shows a closeup of a deposit made from the same concentration as the deposit to its immediate left; in some cases, multiple closeups for a single concentration are shown. The scale bar is 500 μm in (f)–(i) and 250 μm in (j).

ments. At the scale of the whole drop a bull's-eye-like pattern is visible. In (a) there are four well defined concentric rings. In (b) and (c) the interior shows concentric marks but they are qualitatively different from those of (a). In (d) again the inner rings are strong though they are finer, less complete, and less organized than those in (a). The rings shown in (a) and (d) form when the contact line is pinned long enough that a large contact line deposit can form. Thus these

rings chronicle the moments of arrested contact line motion. In contrast, direct observation of the deposition process leading to (b) and (c) shows that the rings in these cases are formed while the contact line is moving.

Magnifying the deposits reveals yet more structure. At the highest concentration [frame (e)], the space between the inner rings is coated by multiple layers of microspheres that are deeper in the vicinity of a ring; the deepening deposit heralds, and perhaps causes, the pinning episode during which a ring is formed. For $\phi = 0.25\%$ [frames (b), (f), and (g)], the interior of the deposit is coated with a layer of microspheres with a thickness that varies between one and two particles. The transition from one- to two-particle layers, indicated by the a steplike increase in brightness, has a saw-toothed shaped pattern pointed radially outward [Fig. 8(f)]. However, the transition from a two- to a one-layer deposit is abrupt, as can be seen from the termination of the outermost saw-toothed front. The saw-toothed front is caused by a piecewise transition to a double layer film. First, a few points along the contact line begin to produce two layers. As the contact line retreats, the segments producing double layers extend along the contact line, leaving a triangular-shaped deposit in their wake. Finally, the segments grow into one another so that the entire contact line deposits double layers. The piecewise growth of the double layer and the abrupt return to a monolayer suggests that there is an energy cost to switching from a single layer to a double layer. If so, the saw-toothed front is an energetically inexpensive means of achieving two-layer production because the distortion energy is localized to a few particle diameters along the contact line.

At $\phi = 0.25\%$ [Fig. 8(g)] and 0.13% [Fig. 8(h)], a gridlike pattern appears. It can exist concurrently with or separately from other patterns at these concentrations. The production of a grid appears to be an unstable version of single-layer production. Direct observation of the contact line shows that parts of it move steadily and that the parts between these move in a stick-slip fashion. The steady moving segments lay down the radial lines of the grid and stick-slip segments produce nothing when moving and a ring when at rest; the combination of the radial lines and the rings forms a grid. Figure 8(i) shows another type of pattern in which single-layer deposition gives way to an even slower rate of deposition that does not achieve total coverage and includes long, empty, radial grooves. Finally, at the lowest concentration ($\phi = 0.063\%$) another new mode appears in which radial spokes are produced [Fig. 8(j)].

B. Patterns with 1-μm particles

[Due to the difficulty of deducing the microscopic behavior of submicron-sized particles with light microscopy, I focused on the behavior of drops with 1-μm particles.] The patterns of deposit left when a drop dries are shown in Fig. 9 for different initial concentrations of 1-μm-sized particles. In Fig. 9, frame (a) is the highest concentration and frame (f) is the lowest. There are distinct features and trends in the deposition patterns. The features may be grouped by distance from the center of the drop. Moving inward, the first zone is a featureless solid packing of particles. This is the initial ring formed before
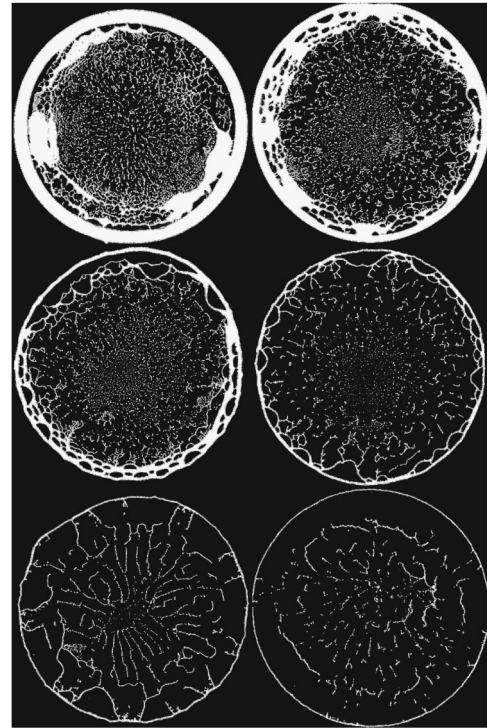

FIG. 9. Deposit left by drops of 1-μm microspheres dried on mica. The initial volume fractions reading from left to right and from top to bottom are 2.0%, 1.0%, 0.5%, 0.25%, 0.13%, and 0.063%. The diameter of each drop is approximately 6 mm.

any depinning has taken place. The second zone consists of arch-shaped formations, the third zone is a mixture of half-formed arches and radial lines, and the central region is composed of apparently disorganized dots. The range of these phases as a function of concentration is plotted in Fig. 10. At high concentration all phases are present but as the concentration decreases, the mixed zone gains at the expense of the others and its composition.

A change in the velocity of the contact line might account for the different phases seen in the deposits. However, direct observation of the contact line shows that there is very little
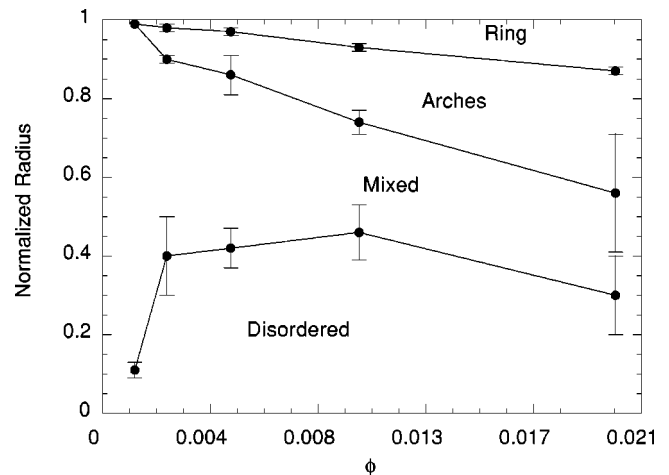

FIG. 10. A diagram indicating the range of each phase: ring, arch, mixed, and disordered phases. The radial position is normalized to 1 at the contact line.
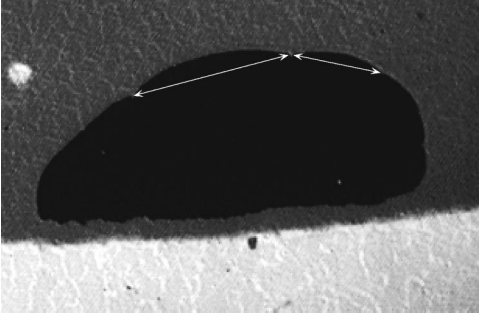
FIG. 11. A closeup view of a large arch shows that it is in fact composed of multiple subarches. The size of these smaller arches was measured as shown.

change in its speed. Another possibility is that the deposition rate at the contact line changes as the drop shrinks. This is consistent with a constant contact line velocity. Moreover, in Ref. [6] we showed that a gradient in the concentration develops and grows while the contact line is pinned. Therefore, the deposition rate would be altered as the contact line moved closer to the origin.

The ring width as a function of concentration was quantified in Sec. III A. Here the focus will be on the other zones beginning first with the arches zone. I measured the size of individual arches from the resulting deposit of many drops; for each concentration a total of approximately 1000 measurements were taken. I took the greatest width of the arch as a measure of its size. Closer inspection of the larger arches showed that they were composed of multiple subarches; for these I measured the width of the subarch rather than width of the entire group. This procedure is shown in Fig. 11. For the first four concentrations represented in Fig. 9, the arch measurements were binned by size and plotted in Figs. 12(a)–12(d). Since there are no arches in drops with $\phi = 0.13\%$, instead I measured the perpendicular distance between spokes where they ran parallel to each other. The distribution function for these measurements is plotted in Fig. 12(e). For the concentration represented by Fig. 9(f) no length scale is apparent, and so no measurements were made. There are two clear trends apparent from the distribution function: for a decreasing concentration the peak of the distribution shifts to a larger value, and the width of the distribution, except for the lowest concentration, grows. The lowest concentration shows an abrupt narrowing of the distribution; this sudden jump corresponds to switching from measuring arch sizes to measuring the distance between radial lines. To extract the trends, the data in Fig. 12 were fit to the functional form $L^{\lambda} \exp(-L/a)$, from which I extracted the peak position and the full width at half height of the distribution. A plot of these parameters is shown in Fig. 13. The change in peak size is well fit by a linear function of concentration.

From observing the processes transpiring at the contact line a partial picture of the pattern formation process emerges. The outermost structure, the ring, was explained briefly in Sec. I and in more detail elsewhere [5,6,9–12]. The arches are formed by the process shown in Fig. 3: a hole is nucleated, the contact line begins to recede, but its growth is arrested by the accumulation of particles. Hole nucleation in nanometer-thick films has been previously observed [13,14],
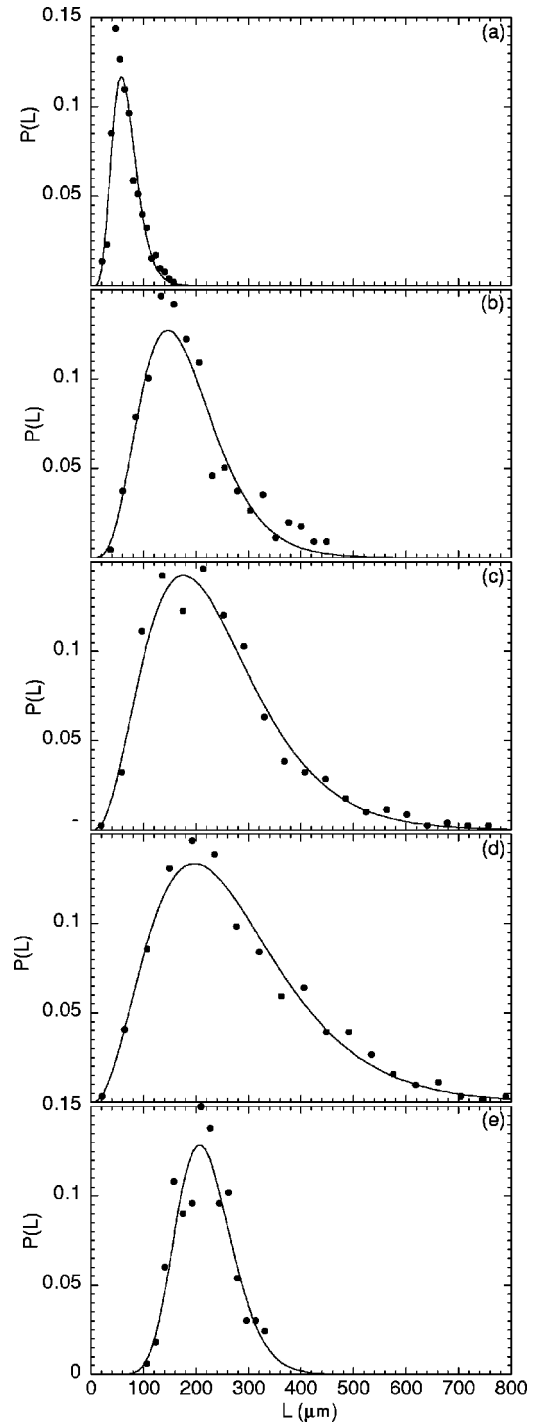

FIG. 12. Plot of the unnormalized distribution function of the arch sizes. Plots (a)–(e) correspond to initial concentrations of 2.0%, 1.0%, 0.5%, 0.25%, and 0.13%, respectively.

and mechanisms for their formation were proposed in Refs. [13] and [15]. However, these mechanisms are inapplicable to the micron-thick films present in my experiments. The growth of arch size with decreasing concentration may be plausibly explained by the fact that there are fewer particles with which to pin the contact line, and this allows the arches to grow larger. By frame (e) of Fig. 9 there is an insufficient number of particles to stop the contact line from moving and the arches grow without bound; this accounts for the absence of arches in frames (e) and (f). Ohara and Gelbart previously
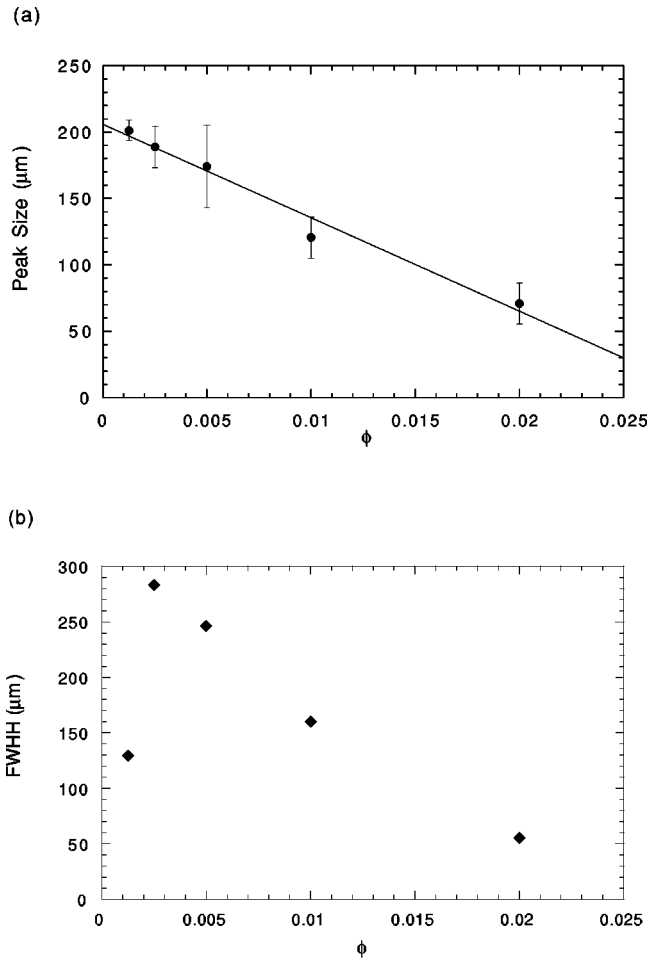
(a)

(b)

FIG. 13. (a) The most likely size of an arch vs concentration taken from the peak position in the curve of Fig. 12. (b) The full width at half height vs concentration of those curves.

proposed the same mechanism for pinning of the contact line by nanoparticles. They predicted that $L \propto 1/\phi$ for a hole spreading in a film of uniform thickness and concentration. The result is not consistent with my data but it is not expected to hold given that a drop is not uniformly thick, that there are additional flows in a ring-forming drops, and that the concentration is not uniform.

The mixed zone begins when the number of holes times their average size becomes comparable to the circumference of the drop. Unlike the arch creation period in which the majority of the contact line is pinned, large portions of the contact line become free to move. At high concentrations this motion is heavily constrained by the accumulation of particles, and is hence erratic. The half-formed arches develop when a small portion of the contact line is temporarily pinned. However, for lower concentrations the contact line organizes itself into a series of cusps that emit particles. This deposition appears to be a release of particles controlled, so that there is no net accumulation at the contact line. During this type of motion, radial lines are formed. The ability of the contact line to do this is thwarted at higher concentrations because the influx of particles is overwhelming. As the concentration is lowered and fewer particles reach the contact line per unit time the ejection process can handle all the particles that arrive; this is the situation in Fig. 9(e). At even
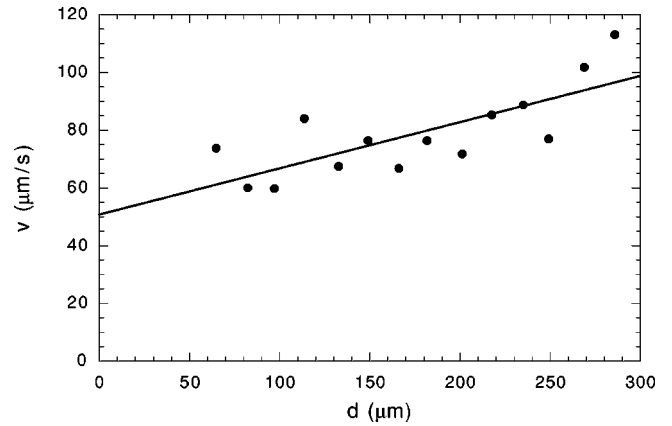

FIG. 14. The velocity of the contact line between two cusps vs the distance between the two cusps. The initial concentration of the drops was $\phi = 6.25 \times 10^{-4}$. The fit is to a linear equation which gives $v = (50.7 + 0.16)d$ in units of μm/s.

lower concentrations [Fig. 9(f)] the output from the cusps can exceed the influx of particles and the emission process becomes discontinuous, leaving disjointed trails of particles which are nonetheless radially oriented.

In other pattern forming systems, such as solidifying alloys, the wavelength selection criterion depends on the velocity of interface. In order to determine if an analogous relation exists in drying drops, I measured the velocity of the minima between two cusps and the cusp-to-cusp distance during the stage when the radial spokes in Fig. 9(e) were generated. The data are plotted in Fig. 14, and they show only a very weak relation between the velocity and the cusp-to-cusp distance.

I also measured the shape of the interface to compare it with the shape expected from contact line elasticity [16] in the low velocity limit. For measurement purposes, I defined the contact line as the outline of the particles caught in the wedge of fluid next to the contact line. Using a fluorescent microscope and fluorescent dyed particles, I captured images of the contact line and extracted the outline of the macroscopic contact line. Since there was no predefined zero, I defined it as the line connecting the lowest point on each side of the cusp. An elaboration of this is shown in Fig. 15. The height of the cusp above the zero line is plotted against distance in Fig. 16, where the zero of the abscissa was chosen to achieve the maximum symmetry between the two sides. The data are well fit by an exponential function. This fit is better than the logarithmic fit expected from contact line elasticity. This discrepancy may be accounted for by viscous dissipation in the fluid, the interaction of the particles through capillary force [17], or deviations from the logarithm due to defect size.

C. Patterns from mixtures

The parameter space of the deposition patterns was further probed by combining colloidal microspheres with surfactant, salt, and microspheres of a different size. A sampling of the results is given below. It is clear that there are many control parameters and that there are many different deposition patterns.
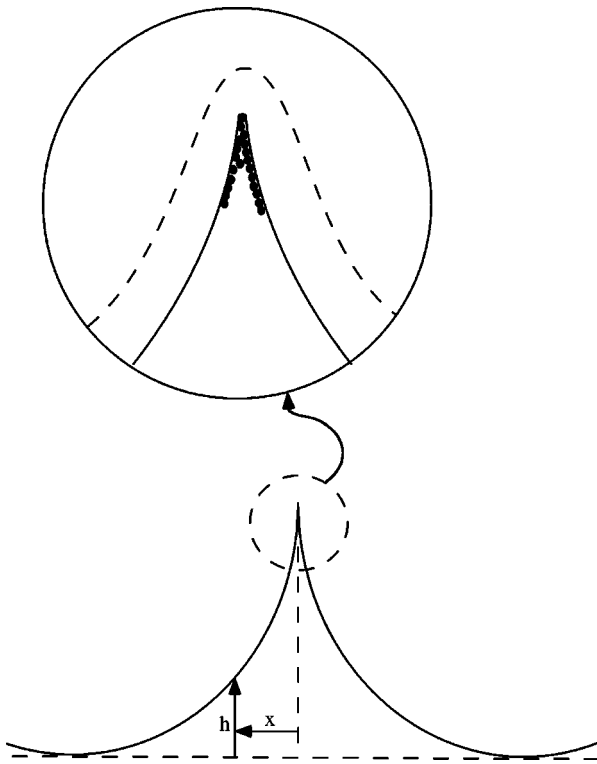
FIG. 15. Schematics for demonstrating the contact line position measurement. The position of the contact line (the dashed line in the closeup) was inferred from the position of the microspheres. The zero height position was chosen as the segment connecting the two minima between a pair of cusps, and the zero x position was chosen by finding the horizontal value at which the left and right hand parts of the curve are most symmetric.

The anionic surfactant sodium dodecyl sulphate (SDS) was added to the 0.1-μm colloid. This was motivated by differences observed in the patterns left by drops of the same concentration but containing colloidal particles synthesized by different manufacturers. By the addition of surfactant to a surfactant-free sample, I was able to produce similar patterns to those formed by other colloid brands. (The inexact match may be due to differences in the ionic strength.) In addition,
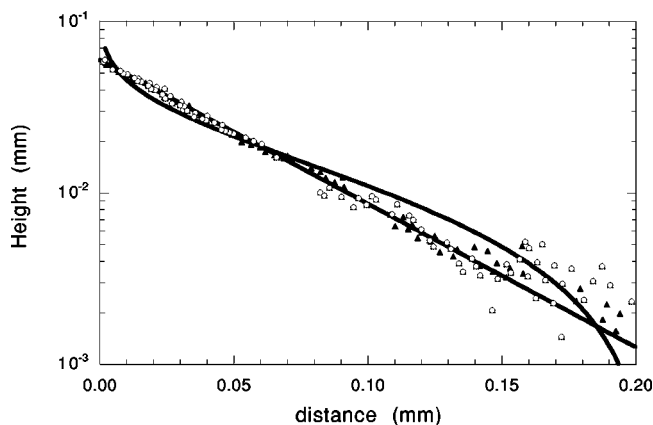

FIG. 16. (c) The position of the contact line relative to the zero point vs distance plotted on a log-linear scale. The straight solid line running through the data is a fit to an exponential, and the curved solid line is a fit to a logarithm.
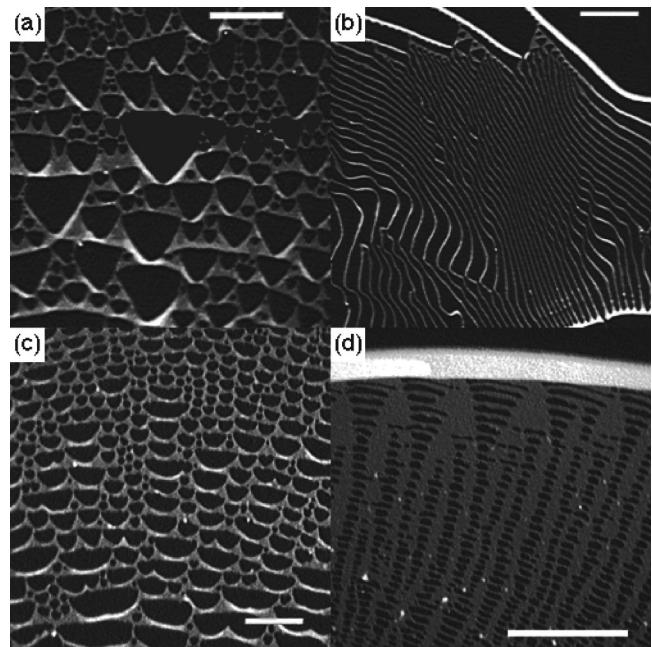

FIG. 17. Deposit left by 0.1-μm microspheres of 0.5% initial volume fraction when a SDS surfactant is added. The center of the drop lies below the image so that the contact line moved from top to bottom. In each image the scale bar corresponds to 50 μm. In frames (a)–(d) the concentration of surfactant is $8.1 \times 10^{-4} M$, $4.3 \times 10^{-4} M$, $1.4 \times 10^{-4} M$, and $4.8 \times 10^{-5} M$, respectively.

I found a number of new patterns which are shown in Fig. 17. These patterns where made from a colloid with a fixed volume fraction of microspheres ($\phi = 0.0013$) but variable concentrations of SDS. During the production of these patterns the contact line sweeps from top to bottom in the images of Fig. 17.

Since the strength and range of the interaction between microspheres and between a microsphere and the substrate is determined by screening ions, I tried altering the ionic strength of the solvent and observed the resulting deposition pattern. Starting with a 2% solid volume-fraction of 1-μm microspheres, I diluted the sample down to $\phi = 0.25\%$ with a NaCl and water solution. The images shown in Fig. 18 are the patterns left when a drop of this mixture is dried on mica. The molarity of the solution used to make (a) was $0M$, (b) was 0.01 mM, (c) was 0.1 mM, and (d) was 1 mM. From these images it is clear that the addition of salt radically alters the resulting deposit. It would be interesting to know if this is due to a change in the particle-particle or particle-substrate interaction, or to the pinning effects of deposited salt.

Last I investigated the effect of combining 0.1- and 1-μm microspheres. Two of the most interesting deposits generated by this binary combination are shown in Fig. 19. These deposits were formed from a one to one mixture of 0.1- and 1-μm colloids with an initial volume fraction of 0.125% and 0.0625%.

IV. CONCLUSION

The major results presented here are that the contact line can self-pin, that the competition between this pinning and dewetting give rise to pattern formation, and that these pat-
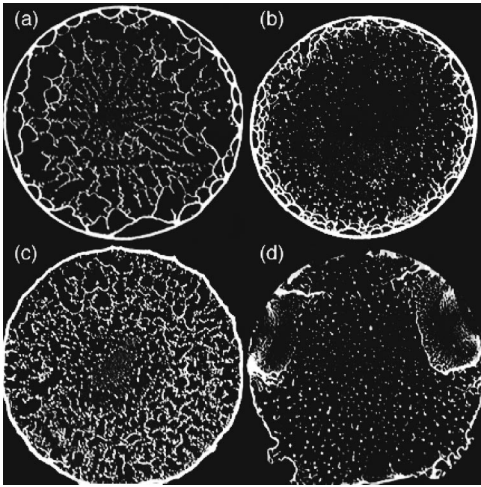
FIG. 18. Deposit left by a 0.25% solid volume-fraction of 1-μm microspheres in a solvent with different ionic strengths (see text). The diameter of the deposits is approximately 6 mm.

terns exhibit evidence of wavelength selection. A drying drop is a new, rich, and unexplored example of a pattern forming system. It can be controlled in numerous ways— solute concentration, particle size, surfactant concentration, ionic strength, and particle mixtures were partly treated here. All the tools that have been developed to treat nonlinear systems far from equilibrium can be brought to bear on this problem. It will be interesting to know if this system fits the standard paradigm of pattern formation.

Investigating pattern formation in drying drops is appealing because a much is already known about contact line behavior and so it ought to be theoretically tractable, and it is a relatively simple experimental system. However, some fundamental experimental and theoretical obstacles must first be tackled. On the experimental side, the circular geometry of a drop is too complicated. The phases shown in Fig. 10 are most likely a manifestation of this problem. In addition, the free drying conditions do not provide sufficient control on the kinetic processes in the system. It is clear that a linear analog of the drop is needed. The result of a simple, well-controlled experiment ought to provide the stimulus that directional solidification and Hele-Shaw experiments provided for moving interface problems [18,19]. Furthermore, the
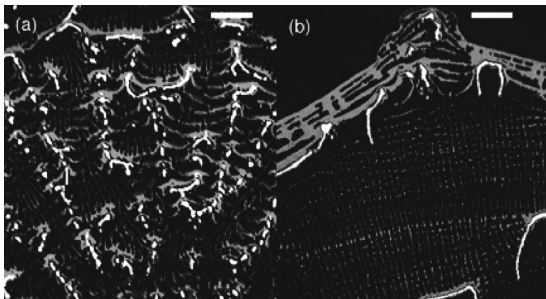

FIG. 19. Deposit left by a 50-50 mixture of 0.1- and 1-μm microspheres diluted down to a volume fraction of 0.125% for (a) and 0.0625% for (b). The bright parts of the deposit correspond to deposits of 1-μm microspheres, and the gray parts correspond to deposits of 0.1-μm microspheres. The scale bar corresponds to 200 μm.
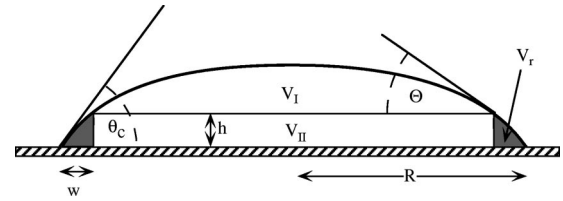

FIG. 20. Diagram depicting the separation of a drop into three regions. Region I is shaped like a spherical cap, and region II is a cylinder. The shape of ring deposit is determined by the equations in the text. At any given time the interface between the ring and the solution is located at w from the contact line and is h high. The aspect ratio is greatly exaggerated.

physical mechanism that drives the retraction of the contact line has yet to be determined.

On the theoretical side, the most obvious unknowns are (1) the flow within a spreading drop of volatile fluid, and (2) the wavelength selection mechanism. The spreading of volatile liquids is a research topic in its own right. However, it appears to be an essential prerequisite for understanding the patterns in drying drops because the flow in the drop determines the distribution of solvent. Though there has been some progress on this spreading problem [20–22], there is as of yet no widely held consensus. The wavelength selection problem is completely open because the result presented here are the first of its kind.

Overall the prospects are good for new ideas about pattern formation emerging from this system. There are a wealth of experimental and theoretical avenues to pursue.

APPENDIX

To model the shape of the deposit at the contact line, and in particular to obtain its width versus time, the drop is separated into three regions (region I, region II, and the ring) as shown in Fig. 20. Regions I and II are composed of solution, and the ring is a solid formed from the solute with packing fraction p. The total volume of liquid at any given moment is

$$V_L = V_I + V_{II} + (1-p)V_r \simeq \pi R^2 h + \frac{\pi R^3 \Theta}{4}, \quad \text{(A1)}$$

where V_r is neglected because it is small compared to V_I and V_{II}, Θ is assumed to be small, and the shape of region I is assumed to be a thin spherical cap. Furthermore, the volume of the drop is assumed to decreases linearly, so that

$$V_L(t) = \frac{\pi R^3 \theta_c}{4}(1 - t/t_f), \quad \text{(A2)}$$

where θ_c is the initial contact angle. From Fig. 20 we obtain the geometrical relation

$$\frac{dh}{dw} = \tan\Theta \simeq \Theta. \tag{A3}$$

The ring grows inward at the rate dw/dt. Therefore, the volume of the ring changes as solute is added and

$$\frac{dV_r}{dt} = 2\pi Rh\frac{dw}{dt}. \tag{A4}$$

Using Eq. (2) gives

$$\frac{dV_r}{dt} = p^{-1}\frac{\pi R^3\theta_0}{4}\phi\frac{(1-(1-t/t_f)^{3/4})^{1/3}}{(1-t/t_f)^{1/4}}. \tag{A5}$$

Putting together Eqs. (A1)–(A5) and introducing the nondimensionalized variables $x \equiv 4w/R$, $y \equiv 4h/(\theta_0 R)$, and τ

$\tau \equiv t/t_f$ we arrive at the pair of coupled ordinary differential equations that govern the shape of the ring:

$$\frac{2\phi}{p}\frac{(1-(1-\tau)^{3/4})^{1/3}}{(1-\tau)^{1/4}} = y\frac{dx}{d\tau}, \tag{A6}$$

$$(1-\tau-y)\frac{dx}{d\tau} = \frac{dy}{d\tau}. \tag{A7}$$

It is clear from the absence of R from nondimensional form of the equations that w will scale with R. For calculation purposes, I assume that $p = 0.656$, and that the initial conditions are that $w(t=0) = 0$ and $h(t=0) = 0$. The equations were integrated numerically to achieve the conversion of the time data in Fig. 4 into the width data displayed in Fig. 5.

[1] T. Young, Philos. Trans. R. Soc. London **95**, 65 (1805).
[2] P. G. de Gennes, Rev. Mod. Phys. **57**, 827 (1985).
[3] E. L. Decker and S. Garoff, Langmuir **13**, 6321 (1997).
[4] R. Johnson and R. Dettre, in *Contact Angle, Wettability and Adhesion*, edited by F. M. Fowkes, Advances in Chemistry Series Vol. 43 (American Chemical Society, Washington, DC, 1964), p. 112.
[5] R. D. Deegan, O. Bakajin, T. F. Dupont, G. Huber, S. R. Nagel, and T. A. Witten, Nature (London) **389**, 827 (1997).
[6] R. D. Deegan, O. Bakajin, T. F. Dupont, G. Huber, S. R. Nagel, and T. A. Witten (unpublished).
[7] G. D. Nadkarni and S. Garoff, Europhys. Lett. **20**, 523 (1992).
[8] Here the ''dewetting'' appellation is meant to encompass all the as-of-yet undetermined forces that drive the contact line to retreat.
[9] F. Parisse and C. Allain, J. Phys. II **6**, 1111 (1996).
[10] F. Parisse and C. Allain, Langmuir **13**, 3598 (1996).
[11] E. Adachi, A. S. Dimitro, and K. Nagayama, in *Film Formation in Waterborne Coatings* edited by T. Provder, M. A. Winnik, and M. W. Urban (American Chemical Society, Washing-

ton, DC, 1996), p. 419.
[12] E. Adachi, A. S. Dimitro, and K. Nagayama, Langmuir **11**, 1057 (1995).
[13] P. C. Ohara and W. M. Gelbart, Langmuir **14**, 3418 (1997).
[14] M. Elbaum and S. G. Lipson, Phys. Rev. Lett. **72**, 3562 (1994).
[15] N. Samid-Merzel, S. G. Lipson, and D. S. Tannhauser, Phys. Rev. E **57**, 2906 (1998).
[16] J. F. Joanny and P. G. de Gennes, J. Chem. Phys. **81**, 552 (1984).
[17] P. A. Kralchevsky, V. N. Paunov, I. B. Ivanov, and K. Nagayama, J. Colloid Interface Sci. **151**, 79 (1992).
[18] J. S. Langer, Rev. Mod. Phys. **52**, 1 (1980).
[19] P. Saffman and G. I. Taylor, Proc. R. Soc. London Ser. A **245**, 312 (1958).
[20] L. M. Hocking, Phys. Fluids **7**, 2950 (1995).
[21] M. Elbaum, S. G. Lipson, and J. S. Wettlaufer, Europhys. Lett. **29**, 457 (1995).
[22] C.-M. Lin, R. M. Ybarra, and P. Neogi, Adv. Colloid Interface Sci. **67**, 185 (1996).